



HAL
open science

Calculation of the steady-state oscillations of a flute model using the orthogonal collocation method

Soizic Terrien, Christophe Vergez, Benoît Fabre, David A.W. Barton

► To cite this version:

Soizic Terrien, Christophe Vergez, Benoît Fabre, David A.W. Barton. Calculation of the steady-state oscillations of a flute model using the orthogonal collocation method. 2013. hal-00903310v1

HAL Id: hal-00903310

<https://hal.science/hal-00903310v1>

Preprint submitted on 11 Nov 2013 (v1), last revised 14 Feb 2014 (v2)

HAL is a multi-disciplinary open access archive for the deposit and dissemination of scientific research documents, whether they are published or not. The documents may come from teaching and research institutions in France or abroad, or from public or private research centers.

L'archive ouverte pluridisciplinaire **HAL**, est destinée au dépôt et à la diffusion de documents scientifiques de niveau recherche, publiés ou non, émanant des établissements d'enseignement et de recherche français ou étrangers, des laboratoires publics ou privés.

Calculation of the steady-state oscillations of a flute model using the orthogonal collocation method

S. Terrien¹⁾, C. Vergez¹⁾, B. Fabre²⁾, D. Barton³⁾

¹⁾ Laboratoire de Mécanique et d'Acoustique, CNRS, UPR 7051, Aix-Marseille Univ, Centrale Marseille, F-13402 Marseille Cedex20, France.

²⁾ LAM, Institut Jean Le Rond d'Alembert, CNRS UMR 7190, UPMC Univ. Paris 6, 11 rue de Lourmel, 75015 Paris, France.

³⁾ Department of Engineering Mathematics, University of Bristol, Bristol, UK.

Abstract

In this paper we exploit the method of numerical continuation combined with orthogonal collocation to analyse the behaviour of a model of a flute-like instrument that is formulated as a nonlinear neutral delay differential equation. The delay term in the model causes additional complications in the analysis of the model, in contrast to models of other wind instruments which are formulated as ordinary differential equations. Fortunately, numerical continuation provides bifurcation diagrams that show branches of stable and unstable solutions of the model and their connections at bifurcations, thus enabling an in depth analysis of the global dynamics. Furthermore, it allows us to predict the thresholds of the different registers of the flute-like instrument and thus to explain the classical phenomenon of register change and the associated hysteresis.

1 Introduction

Flute-like musical instruments present complex behaviour, some aspects of which remain poorly understood. The study of a physical model of this instrument class provides the opportunity to explore the influence of different parameters and, by comparison with experimental results, to improve the knowledge of the physical mechanisms of sound production.

Many studies have dealt with the calculation of self-sustained oscillations of flute models. Time-domain simulations (see for example [1, 2, 3]) allow the computation of both transients and steady-state periodic and non-periodic oscillations, and are thus informative about the diver-

sity of dynamical regimes. Nevertheless, these methods are very sensitive to initial conditions, and do not necessarily provide information about coexistence of multiple solutions. Some analytical methods were proposed by Schumacher and Fletcher [4, 5], but require drastic simplifications of the model. Moreover, due to both their complexity and the limitation to a few number of harmonics, these methods are not suited for a systematic study of the instrument behaviour.

Numerical methods for the calculation of periodic solutions of nonlinear dynamical systems have been developed for decades in the field of nonlinear differential equations: they include in particular the harmonic balance method (HBM), based on a frequency-domain discretization of the solution (see for example [6]), and the orthogonal collocation method [7, 8], based on a time-domain discretization.

Since they can be combined with *numerical continuation methods* [9], these techniques are particularly interesting. Indeed, the HBM or the orthogonal collocation considered alone compute periodic solutions for different values of the model parameters (see figure 1-(a)), each point being independent from the others. Numerical continuation methods rely on the implicit function theorem (see for example [9]) to say that these points lie on a continuous solution branch. Therefore, they can follow the evolution of a given periodic solution in a $\lambda - x$ plane, leading to a branch of periodic solutions, as represented in figure 1-(b).

The computation of the different branches leads to bifurcation diagrams, which represent static and periodic solutions of the model, as a function of a parameter of interest (the so-called continuation parameter). Since bifurcation diagrams

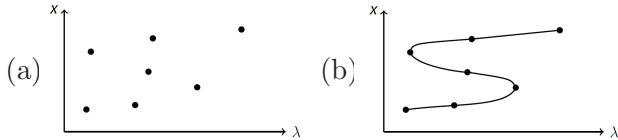


Figure 1: Schematic representation of the principle of numerical continuation. (a): periodic solutions x obtained through, for example, orthogonal collocation, represented as a function of the parameter λ . (b): branch of periodic solution obtained through numerical continuation.

give information about the coexistence of multiple solutions and the presence of unstable solutions, such diagrams provide a more global knowledge of the system dynamics.

For the first time in 1989, the harmonic balance method was introduced in musical acoustics by Gilbert et al. [10]. This technique has then been used in various works focusing on single reed musical instruments [11, 12, 13] and brass instruments [14, 15]. Recent studies [16, 17] have then demonstrated the benefits of combining this technique with numerical continuation methods to understand the behaviour of clarinet-like instruments. In parallel, software packages have been developed (among which [8, 18, 19, 20]), that combine periodic solution computations and numerical continuation methods.

Compared to models of other wind instruments, the state-of-the-art model for flute-like instruments contains an additional delay term due to the presence of an air jet in the excitation mechanism, and is moreover a neutral delayed dynamical system (that is to say it includes a delay in the highest derivative - see section 2). Such systems are mathematically more complex than ordinary differential equations governing, for example, the behaviour of reed instruments. In principle, the harmonic balance method can be used to solve this kind of systems [21]. However, the current work does not aim to develop from scratch a new software package specifically dedicated to the flute model, but rather to take advantage of existing validated numerical tools. Nevertheless, the different numerical tools cited above do not allow calculation and continuation of periodic solutions of neutral equations, and the associated numerical schemes must be adapted.

A first attempt to study flute-like instruments through numerical continuation, using a toy-model (mathematically a more simple non-neutral

delayed dynamical system), has highlighted that such an approach provides new kind of information, explaining behaviours which can be related to some experimental phenomena [22]. It thus suggests to study the state-of-the-art model of flute-like instruments in the same way, and therefore to introduce numerical tools adapted to neutral systems. This is done thanks to the contribution of Barton [23], whose work allows the analysis of neutral systems within the DDE-Biftool environment.

We first recall in section 2 the equations of the state-of-the-art physical model of flute-like instruments. We then describe in section 3 the orthogonal collocation method and the predictor-corrector approach, which respectively allow the computation and the continuation of periodic solutions of neutral delay dynamical systems. Finally, an application to the model of flute-like instruments highlights in section 4 the valuable contribution of such an approach to the understanding of the phenomenon of "register change" and its associated hysteresis, two typical features of flute-like instruments.

2 State-of-the-art model for flutes

As for other wind instruments, the establishment of auto-oscillation in flute-like instruments results from the coupling between an exciter and a resonator constituted by the air column contained in the pipe. The peculiarity of flute-like instruments lies in the nature of the exciter. Whereas the excitation mechanism of other wind instruments involves the vibration of a solid element (such as a cane reed or the musician's lips), it is constituted here by the nonlinear interaction of an air jet with a sharp edge called "labium" (see figure 2).

More precisely, when the musician blows in the instrument, a jet of velocity U_j and semi-half width b is created at the exit of a channel which is a part of the instrument in the case of recorders or flue organ pipes, as highlighted in figure 2, and formed by the player's lips for transverse flutes. As the jet is naturally unstable, any perturbation is amplified while convected along the jet, from the channel exit to the labium. The convection velocity c_v of these perturbations on the jet is related to the jet velocity itself through: $c_v \approx 0.4 U_j$ [24, 25, 26]. The jet-labium interaction then

makes the jet oscillate around the labium with a deflection amplitude $\eta(t)$ (see figure 3), leading to an alternate flow injection inside and outside the instrument. The mass of air contained between these two flow sources in phase opposition (separated by a small distance δ_d , whose value is evaluated by Verge in [27]) acts as a dipolar pressure source $\Delta p_{src}(t)$ on the air column contained in the pipe [28, 27, 29], which constitutes the resonator, represented through its input admittance Y_{in} . The acoustic velocity $v_{ac}(t)$ of the waves created in the resonator disrupts back the air jet at the channel exit. As described above, this perturbation is convected and amplified along the jet, toward the labium (see figure 3). The duration of convection introduces a delay τ in the system, related both to the distance W between the channel exit and the labium (see figure 2) and to the convection velocity c_v through: $\tau = \frac{W}{c_v}$. The instability is amplified through this feedback loop, leading to self-sustained oscillations.

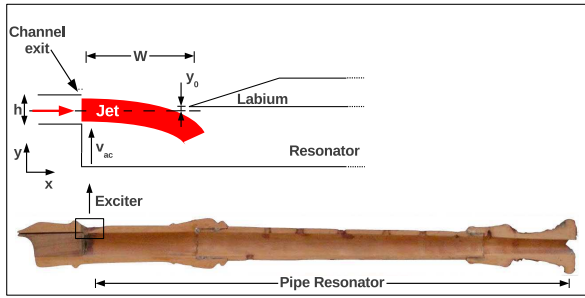


Figure 2: Recorder section, and simplified representation of the jet oscillation around the labium, in the mouth of the resonator.

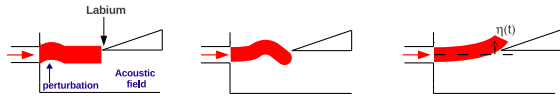


Figure 3: Schematic representation of the jet behaviour, based on Fabre in [30].

This mechanism of sound production can be represented by a feedback loop system, represented in figure 4.

According to various studies describing the different physical phenomena involved ([24, 25, 26, 31, 32] for the jet, [28, 27, 29] for the aeroacoustic source), the state-of-the-art model for flute-like instruments is described through system 1, whose

each equation is related to a given element of the feedback loop system of figure 4.

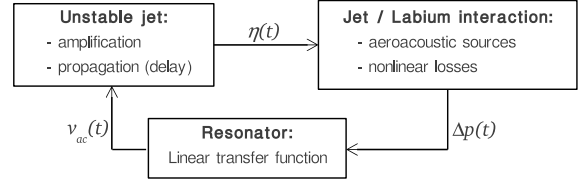


Figure 4: Basic modeling of sound production mechanism in flute-like instruments, as a system with a feedback loop [30, 33].

$$\begin{aligned} \eta(t) &= \frac{h}{U_j} e^{\alpha_i W} v_{ac}(t - \tau) \\ \Delta p(t) &= \Delta p_{src} + \Delta p_{los} \\ &= \frac{\rho \delta_d b U_j}{W} \frac{d}{dt} \left[\tanh \left(\frac{\eta(t) - y_0}{b} \right) \right] \\ &\quad - \frac{\rho}{2} \left(\frac{v_{ac}(t)}{\alpha_{vc}} \right)^2 \text{sgn}(v_{ac}(t)) \end{aligned} \quad (1)$$

$$\begin{aligned} V_{ac}(\omega) &= Y_{in}(\omega) \cdot \Delta P(\omega) \\ &= \left[\frac{a_0}{b_0 j \omega + c_0} + \sum_{k=1}^{p-1} \frac{a_k j \omega}{\omega_k^2 - \omega^2 + j \omega \frac{\omega_k}{Q_k}} \right] \cdot \Delta P(\omega) \end{aligned}$$

In these equations, α_i is an empirical coefficient characterizing the amplification of the jet perturbations [24, 31], ρ is the air density, and y_0 the offset between the labium position and the jet centerline (see figure 2). V_{ac} and ΔP are respectively the frequency-domain expressions of the acoustic velocity at the pipe inlet and the pressure source.

In the second equation, the additional term $\Delta p_{los} = -\frac{\rho}{2} \left(\frac{v_{ac}(t)}{\alpha_{vc}} \right)^2 \text{sgn}(v_{ac}(t))$ models nonlinear losses due to vortex shedding at the labium [34]. α_{vc} is a *vena contracta* factor (estimated at 0.6 in the case of a sharp edge), and sgn represents the sign function.

The input admittance $Y_{in}(\omega)$ is represented in the frequency-domain as a sum of resonance modes, including a mode at zero frequency (the so-called uniform mode [30]). The coefficients a_k , ω_k and Q_k are respectively the modal amplitude, the resonance pulsation and the quality factor of the k^{th} resonance mode, ω is the pulsation, and a_0 , b_0 and c_0 are the coefficient of the uniform mode.

A reformulation of system (1) as a classical first-order system:

$$\dot{x}(t) = f(x(t), x(t - \tau), \dot{x}(t - \tau), \lambda) \quad (2)$$

is helpful to highlight the mathematical nature of the model, and necessary for its implementation in DDE-Biftool. In such a formulation, x is the vector of state variables, λ the set of parameters, and f a nonlinear function. In order to improve numerical conditioning, the system under study is made dimensionless through the definition of the following dimensionless variables:

$$\begin{aligned} \tilde{t} &= \omega_1 t \\ \tilde{v}(\tilde{t}) &= \frac{h e^{\alpha_i W}}{b U_j} v_{ac}(\tilde{t}). \end{aligned} \quad (3)$$

The development is detailed in appendix A, and finally leads to the following system of $2p-1$ equations (with p the total number of acoustic modes in the third equation of system (1)):

$$\begin{aligned} \dot{\tilde{v}}_0(\tilde{t}) &= \frac{a_0 \rho \delta_d h e^{\alpha_i W}}{W b_0} \sum_{i=0}^{p-1} \tilde{z}_i(\tilde{t} - \tilde{\tau}) \\ &\quad \left\{ 1 - \tanh^2 \left[\sum_{i=0}^{p-1} \tilde{v}_i(\tilde{t} - \tilde{\tau}) - \frac{y_0}{b} \right] \right\} \\ &\quad - \frac{a_0 \rho b W}{2 b_0 \alpha_{vc}^2 h e^{\alpha_i W} \gamma \tilde{\tau}} \sum_{i=0}^{p-1} \tilde{v}_i(\tilde{t}) \\ &\quad \text{abs} \left(\sum_{i=0}^{p-1} \tilde{v}_i(\tilde{t}) \right) - \frac{c_0}{b_0 \omega_1} \tilde{v}_0(\tilde{t}) \\ \dot{\tilde{v}}_k(\tilde{t}) &= \tilde{z}_k(\tilde{t}) \\ \dot{\tilde{z}}_k(\tilde{t}) &= \frac{a_k \rho \delta_d h e^{\alpha_i W}}{W} \sum_{i=0}^{p-1} \dot{\tilde{z}}_i(\tilde{t} - \tilde{\tau}) \\ &\quad \left\{ 1 - \tanh^2 \left[\sum_{i=0}^{p-1} \tilde{v}_i(\tilde{t} - \tilde{\tau}) - \frac{y_0}{b} \right] \right\} \\ &\quad - \frac{2 a_k \rho \delta_d h e^{\alpha_i W}}{W} \left(\sum_{i=0}^{p-1} \tilde{z}_i(\tilde{t} - \tilde{\tau}) \right)^2 \\ &\quad \tanh \left[\sum_{i=0}^{p-1} \tilde{v}_i(\tilde{t} - \tilde{\tau}) - \frac{y_0}{b} \right] \\ &\quad \left\{ 1 - \tanh^2 \left[\sum_{i=0}^{p-1} \tilde{v}_i(\tilde{t} - \tilde{\tau}) - \frac{y_0}{b} \right] \right\} \\ &\quad - \frac{a_k \rho b W}{2 \alpha_{vc}^2 h e^{\alpha_i W} \gamma \tilde{\tau}} \sum_{i=0}^{p-1} \tilde{z}_i(\tilde{t}) \\ &\quad \text{abs} \left(\sum_{i=0}^{p-1} \tilde{v}_i(\tilde{t}) \right) - \left(\frac{b W}{\gamma \tilde{\tau} \alpha_{vc} h e^{\alpha_i W}} \right)^2 \\ &\quad \frac{a_k \rho \omega_1}{2} \sum_{i=0}^{p-1} \tilde{v}_i(\tilde{t}) \sum_{i=0}^{p-1} \tilde{z}_i(\tilde{t}) \\ &\quad \text{sgn} \left(\sum_{i=0}^{p-1} \tilde{v}_i(\tilde{t}) \right) - \left(\frac{\omega_k}{\omega_1} \right)^2 \tilde{v}_k(\tilde{t}) \\ &\quad - \frac{\omega_k}{\omega_1 Q_k} \tilde{z}_k(\tilde{t}) \end{aligned} \quad (4)$$

$\forall k \in [1; 2; \dots; p-2; p-1]$.

Such a formulation highlights the presence of a delayed derivative term $\dot{\tilde{z}}(\tilde{t} - \tilde{\tau})$, and thus the neutral nature of the system, already underlined in [3, 35].

This feature of the model constitutes an important difference with other wind instruments (such as reed instruments and brass instruments), which are modeled through ordinary differential equations.

3 Methods: orthogonal collocation and numerical continuation

Since the early works of Gilbert *et al* [10] about the determination of periodic solutions of self-sustained systems, different numerical tools have been developed or adapted to perform such calculations for musical instruments models.

Particularly, different studies have dealt with both computation and continuation of periodic solutions and bifurcation analysis of reed instruments with the software AUTO [16], Harmbal [12, 11] or Manlab [18, 17]. These software differ in numerical methods they use, both for the calculation of periodic solutions (harmonic balance and collocation for Manlab, collocation for AUTO), and for the continuation algorithm (predictor-corrector method for AUTO, asymptotic numerical method for Manlab).

As underlined in the previous section and in [3], even the simplest model of flute-like instrument includes an additional delay compared to models of other wind instruments. As they do not deal with delayed differential equations, the different software mentioned above are not helpful for the present study. Among the few distributed numerical tools dealing with computation and continuation of periodic solutions in delayed systems, as Knut [36] and DDE-Biftool [19], only DDE-Biftool has been subsequently adapted to treat the case of neutral delayed differential equations [23, 37]. Throughout this paper, numerical results are thus computed using DDE-Biftool and its extension for neutral systems, both based on orthogonal collocation method [38, 23, 39] for computation of periodic solutions and on a predictor-corrector approach for continuation of solution branches. The general principles of orthogonal collocation, and its extension to neutral delayed equations are thus briefly recalled below.

3.1 Principles of the method

Numerical resolution of a system of ordinary, delayed or neutral differential equations implies a discrete representation of the unknown solution. Orthogonal collocation method allows to compute periodic solutions, based on a temporal discretisation of a single period. As we are interested in self-oscillating systems, it is important to note that the period T of the solution is an unknown

of the problem. The principle of the method used here consists in approximating the real solution by a piecewise polynomial.

More precisely, a single (unknown) period of the periodic solution is divided in N intervals, which constitutes a mesh Π :

$$\Pi = [t_0 = 0; t_1; t_2; \dots; t_{N-1}; t_N = T]. \quad (5)$$

The number N of intervals considered influences on the results accuracy.

Each interval $[t_i; t_{i+1}]$ is again discretised on a set of $m+1$ *representation points*, distributed uniformly on the interval. On each interval, the solution is interpolated by Lagrange polynomials. On an interval defined as $t \in [t_i; t_{i+1}]$, the approximate solution $\hat{x}(t)$ of the real solution $x(t)$ is thus defined as:

$$\hat{x}(t) = \sum_{j=0}^m x_{i+\frac{j}{m}} \cdot P_{i,j}(t) \quad (6)$$

where $x_{i+\frac{j}{m}}$ is the value of the solution at the representation point $t_{i+\frac{j}{m}} = t_i + \frac{j}{m}(t_{i+1} - t_i)$, and $P_{i,j}(t)$ the Lagrange interpolating polynomial, defined as:

$$P_{i,j}(t) = \prod_{r=0; r \neq j}^m \frac{t - t_{i+\frac{r}{m}}}{t_{i+\frac{j}{m}} - t_{i+\frac{r}{m}}} \quad (7)$$

The unknowns are thus the values of $x_{i+\frac{j}{m}}$, and the period T . Taking into account the continuity conditions at the mesh points t_i , one obtains, for a L -dimensional system, $L(Nm + 1) + 1$ unknowns.

For each interval, the equations are not written at the $m+1$ representation points, but at the m *collocation points*, defined as the zeros of the m -order Legendre polynomial for the considered interval. This choice of collocation points gives an optimal rate of convergence as the number of mesh points increases. Projection of the differential equations on these $N \times m$ collocation points leads to an algebraic system of NmL equations. The $L + 1$ additional equations required to close the system are provided by the periodicity condition: $x(0) = x(T)$ (L equations) and by a phase condition. Indeed, as the solutions are periodic, if $x(t)$ is a solution, $x(t + \phi)$ is also a solution, regardless the value of ϕ . A phase condition is therefore introduced to fix the phase origin. A very common choice, adopted here, is the *integral phase condition*, initially introduced by Doedel [8].

3.2 Adaptation of the method to neutral delay systems

The extension of orthogonal collocation method to neutral delayed differential equations, imposes to define an interpolation scheme for the approximation of both the delayed and the derivative delayed variables. Various schemes have been proposed for the case of non-neutral delayed systems, as for example in [38]. For the case of neutral systems, Barton [23] proposed the following approximations, implemented in the extension of DDE-Biftool for neutral equations:

$$\begin{aligned}\widehat{x}(t-\tau) &= \sum_{j=0}^m x_{k+\frac{j}{m}} \cdot P_{k,j}(t) \\ \widehat{\dot{x}}(t-\tau) &= \sum_{j=0}^m x_{k+\frac{j}{m}} \cdot P'_{k,j}(t)\end{aligned}\quad (8)$$

where $P_{k,j}(t)$ corresponds to the Lagrange interpolating polynomial defined in equation (7), and $P'_{k,j}(t)$ to its derivative. k is an integer such that $(t-\tau) \in [t_k; t_{k+1}]$. For more details, we refer the reader to [23] and [37].

3.3 Stability of static and periodic solutions

Let us consider the following system of neutral differential equations:

$$\dot{x}(t) = f(x(t), x(t-\tau), \dot{x}(t-\tau), \lambda). \quad (9)$$

For sake of clarity, we consider here a system with a single delay, but the following considerations can be generalised to multi-delay systems.

A static solution x_s of system (9) satisfies the following equation:

$$f(x_s, x_s, 0, \lambda_s) = 0. \quad (10)$$

Stability property of such an equilibrium solution is given by the stability of equation (9) linearised around the considered static solution x_s :

$$\dot{x}(t) = A_0 [x(t) - x_s] + A_1 [x(t-\tau) - x_s] + A_2 \dot{x}(t-\tau) \quad (11)$$

where A_i is the partial derivative of the nonlinear function f with respect to its $(i+1)^{th}$ argument. Defining a new variable $y(t) = x(t) - x_s$, equation (11) becomes:

$$\dot{y}(t) = A_0 y(t) + A_1 y(t-\tau) + A_2 \dot{y}(t-\tau). \quad (12)$$

The stability of this linearised equation depends on the value of the roots κ of its associated characteristic equation:

$$\det(\kappa I - A_0 - A_1 e^{-\kappa\tau} - \kappa A_2 e^{-\kappa\tau}) = 0 \quad (13)$$

where I is the identity matrix. This transcendental equation has an infinite number of roots, and its resolution requires specific numerical techniques (see for example [40]).

If all the roots κ have negative real parts, any disturbance of the equilibrium solution is attenuated with time, and the solution is locally stable. Conversely, if at least one of these eigenvalues has a positive real part, a small disturbance superimposed on the solution is amplified with time, and the solution is thus locally unstable. We precise *local* stability because this calculation involves the linearisation of the system around a solution, and the analysis is thus only valid for small perturbations around the considered solution. Further details and demonstrations are provided in [9, 40].

When a stable equilibrium solution becomes unstable, the system behaviour after this *bifurcation point* depends on the real, pure imaginary or complex feature of the eigenvalue which crosses the imaginary axis (see for example [41]).

Throughout this paper, we particularly focus on the case where two complex conjugate eigenvalues cross the imaginary axis. This scenario corresponds to a Hopf bifurcation, which gives rise to a periodic solution, and is thus particularly interesting in the case of musical instruments.

This local stability analysis can be generalised to periodic solutions (see [41]), whose stability properties then depends on the eigenvalues of the *monodromy operator*, the so-called *Floquet multipliers* [41, 9]. A periodic solution is stable as long as all its Floquet multipliers lie in the unit circle. As previously, when a periodic solution loses its stability, the resulting regime observed after this bifurcation point depends on which way the Floquet multipliers leave the unit circle at the bifurcation point.

3.4 Continuation method

Starting from a static or periodic solution x_0 computed for a set of parameters λ_0 , numerical con-

tinuation methods allow (under sufficient conditions on the smoothness of the nonlinear function f) to follow the solution when a parameter - the continuation parameter - varies. Thus, one can access to a solution family (x, λ) , called *branch of solutions*, which contains the solution (x_0, λ_0) . As underlined for example in [16], different numerical continuation methods exist: one can cite classical predictor-corrector methods, which rely on a discrete representation of the branches, and the asymptotic numerical method [18], which attempts to compute continuous portions of the solution branches.

The software DDE-Biftool, used for the present study, uses a predictor-corrector continuation algorithm: knowing a point (x_0, λ_0) of a branch, the neighboring point (for a set of parameter $\lambda_0 + \Delta\lambda$) is first estimated through a secant predictor [9, 19], and then corrected using an iterative Newton-Raphson algorithm. This process thus allows to compute the whole solution branch.

To improve numerical conditioning, and avoid the common but pathological case of a vertical tangent - which corresponds to a fold (or saddle-node) bifurcation [41] - the solution branch is parameterised through the Keller pseudo-arclength equation, which can be seen as a kind of curvilinear abscissa. For more details, we refer the reader to [42].

Numerical continuation algorithm, coupled to the orthogonal collocation method, can be used to calculate bifurcation diagrams of the system of interest. In an ideal case, such diagrams show all the static and periodic solutions as a function of the *continuation parameter*. Through knowledge of unstable solutions, coexistence of solutions, and bifurcations of periodic solutions, it provides a more global vision of the system dynamics than time-domain simulations alone. However, computation of a solution branch through numerical continuation requires the knowledge of at least a point of this branch (i.e. a *starting point*), which raises the question of initialisation. It is thus impossible to be sure that a *complete* bifurcation diagram has been obtained.

4 Application to flute-like instruments

4.1 Comparison of the results with time-domain simulations

In order to validate the continuation approach, we first focus on the comparison, in terms of amplitude, frequency and waveforms, between the results of a classical time-domain solver based on a Runge-Kutta method on the one hand and the bifurcation diagram on the other hand.

As it is directly related to the pressure in the musician's mouth (and thus to the choice of whether that he blows hard or not), the dimensionless delay $\tilde{\tau}$ is a particularly interesting parameter, and is chosen as bifurcation parameter.

Parameter values used for the different calculations are summarised in table 1. We consider here the ideal case of a cylindrical resonator without side holes, 400 mm in length and 16 mm diameter, which is close to the typical dimensions of an alto recorder. The contribution of the excitation window is taken into account through a correction term in the analytical formula of the input admittance (see [30] for more details). From the input admittance calculated analytically, a fitting algorithm allows the extraction of the modal coefficients of the six first resonance modes. The comparison, in terms of modulus and phase, between the original and the fitted admittances, is provided in figure 5. One can note that an increase of the number of modes taken into account allows a better modeling of the input admittance. However, the system dimension being directly related to the number of modes, adding modes considerably increases the computation cost. Since the amplitude of the higher order modes is considerably smaller than that of the first mode, the number of six modes seems to be a reasonable compromise.

For sake of clarity, we first consider a single periodic solution branch, corresponding to the second register, that is to say to oscillations at a frequency close to the second resonance frequency of the input admittance.

Figure 6 represents the amplitude of the acoustic velocity v_{ac} as a function of the dimensionless delay $\tilde{\tau}$, for both the results obtained through time-domain integration for three fixed $\tilde{\tau}$ values ($\tilde{\tau} = 0.6$, $\tilde{\tau} = 0.846$ and $\tilde{\tau} = 1.2$) and the branch computed thanks to numerical continuation algo-

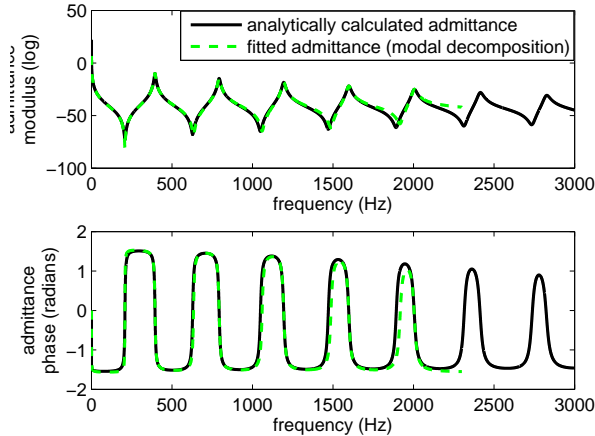


Figure 5: Analytically calculated and fitted input admittances of a cylindrical resonator of flute-like instrument, 400 mm in length and 16mm diameter.

rithm. Since it leads to convergence of the solver and permits an easy resampling of the signals at a sampling frequency suitable for audio production systems, a sampling frequency $f_s = 10 \times 44100$ Hz is used for time-domain simulations. Orthogonal collocation is achieved using 75 mesh points per period, and an interpolation polynomial of degree 5. This comparison shows good agreement between the results of the two methods, with a maximum relative deviation of the amplitude of 0.36 % at $\tilde{\tau} = 1.2$.

Figure 7 provides, for the same data, the comparison in terms of oscillation frequency. As for the amplitude, this comparison shows good agreement, with a maximum relative deviation of 0.1 % at $\tilde{\tau} = 0.6$, which corresponds to 1.7 cent.

Figure 7 provides, for the same data, the comparison in terms of oscillation frequency. As for the amplitude, this comparison shows good agreement, with a maximum relative deviation of 0.1 % at $\tilde{\tau} = 0.6$, which corresponds to 1.7 cent.

In the same way, figure 8 provides the comparison between the two methods, for both the calculated waveforms and amplitude of the 15 first harmonics of the spectrum, at the three different points of the branch already represented in figure 6. Although the sampling frequency used for simulations and the number of discretisation points retained for orthogonal collocation are not "equivalent" (and thus the two methods do not resolve the same number of harmonics), these comparisons show again good agreement. Especially, the calculation of the L2-norm of the different

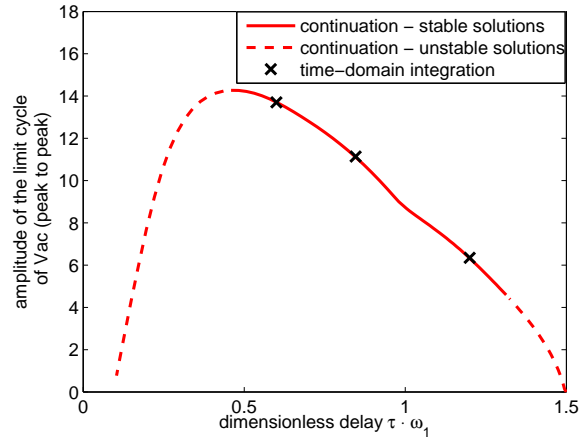


Figure 6: Oscillation amplitude as a function of the dimensionless delay $\tilde{\tau}$ for a single periodic solution branch : comparison between the results of numerical continuation and time-domain integration.

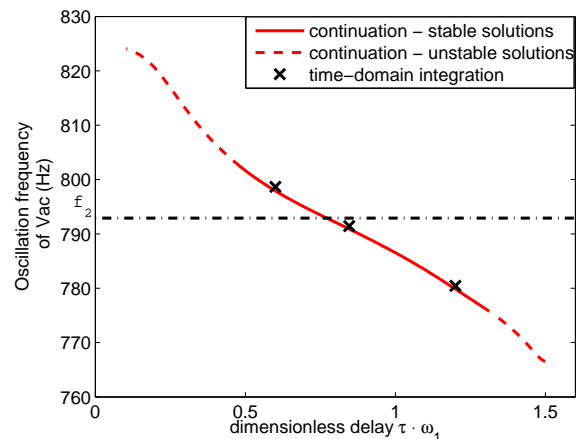


Figure 7: Oscillation frequency as a function of the dimensionless delay $\tilde{\tau}$ for a single periodic solution branch : comparison between the results of numerical continuation and time-domain integration. The dark dot-dashed line indicates the second resonance frequency ($f_2 = \frac{\omega_2}{2\pi}$) of the resonator.

Parameter	Numerical value
a_0 ($\text{m}^2 \cdot \text{kg}^{-1}$)	642
b_0	83
c_0 (s^{-1})	294
a_1 ($\text{m}^2 \cdot \text{kg}^{-1}$)	15
ω_1 ($\text{rad} \cdot \text{s}^{-1}$)	2480
Q_1	50
a_2 ($\text{m}^2 \cdot \text{kg}^{-1}$)	14
ω_2 ($\text{rad} \cdot \text{s}^{-1}$)	4982
Q_2	64
a_3 ($\text{m}^2 \cdot \text{kg}^{-1}$)	12
ω_3 ($\text{rad} \cdot \text{s}^{-1}$)	7501
Q_3	72
a_4 ($\text{m}^2 \cdot \text{kg}^{-1}$)	10
ω_4 ($\text{rad} \cdot \text{s}^{-1}$)	10040
Q_4	77
a_5 ($\text{m}^2 \cdot \text{kg}^{-1}$)	9
ω_5 ($\text{rad} \cdot \text{s}^{-1}$)	12595
Q_5	77
α_i (m^{-1})	$0.4/h = 400$
δ_d (m)	$\frac{4}{\pi} \sqrt{(2hW)} = 0.0036$
b (m)	$2h/5 = 0.0004$
y_0 (m)	0.0001
h (m)	0.001
W (m)	0.0425
ρ ($\text{kg} \cdot \text{m}^{-3}$)	1.2
c_p ($\text{m} \cdot \text{s}^{-1}$)	$0.4U_j$
α_{vc}	0.6

Table 1: Parameter values used for numerical resolutions of the model.

waveforms highlights relative deviations between the results of orthogonal collocation and time-domain simulation of 0.78% at $\tilde{\tau} = 0.6$, 0.46% at $\tilde{\tau} = 0.846$ and 0.04% at $\tilde{\tau} = 1.2$.

Although these results focus on a single solution branch, and thus lead to a very partial knowledge of the model behaviour, they nevertheless provide, compared to more classical analysis and resolution methods (such as linear analysis and time-domain simulations), new information about the functioning of the instrument. For sake of consistency with the literature, oscillation amplitude and frequency (already represented respectively in figures 6 and 7) are represented in figures 9 and 10 as functions of the reduced jet velocity θ :

$$\theta = \frac{U_j \cdot 2\pi}{W\omega_1}. \quad (14)$$

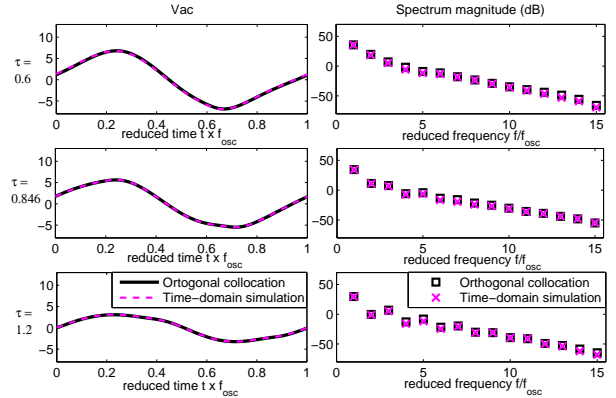


Figure 8: Comparison between the results of orthogonal collocation and time-domain integration in terms of waveform (left) and spectrum magnitude (right). Each line corresponds to a value of $\tilde{\tau}$ ($\tilde{\tau} = 0.6$ for the first line, $\tilde{\tau} = 0.846$ for the second line, $\tilde{\tau} = 1.2$ for the third line).

Such representations shed some light on different known behaviours of the instrument. Especially, it highlights that the methods used here predict precisely the saturation of the oscillation amplitude (figure 9), a commonly observed behaviour in experiments and simulations [1, 5, 43, 3], which is not explained or predicted by the often-used linear analysis of the model [3]. In the same way, if the strong dependence of the frequency on the jet velocity U_j , highlighted in figure 10, is a well-known behaviour of both models and real instruments (see for example [44, 1, 43, 3, 22, 45]), a linear analysis of the model only gives a rough estimation of the frequency evolution, and does not distinguish between stable and unstable parts of the branch. As highlighted in figure 10, the bifurcation diagram not only predicts precisely the frequency evolution along the branch, but also the stabilisation of the frequency slightly above the resonance frequency [3]. Through the computation of stability properties of the branch of periodic solutions, it finally gives information about the minimum and maximum frequencies that can be observed for a given periodic regime. Thereby, figure 10 highlights that the oscillation frequency of the second register can evolve between 776 Hz (at $\theta = 12$) and 804 Hz (at $\theta = 34$), whereas a linear analysis would merely give an estimation of the frequency at the branch extremities (here at $\theta = 10.5$ and $\theta = 152$).

To conclude, this first study of a single branch

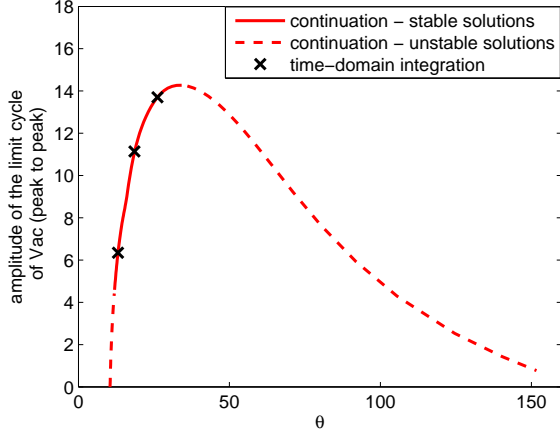


Figure 9: Oscillation amplitude as a function of the reduced jet velocity θ for a single periodic solution branch. Superimposition of the results of numerical continuation and time-domain integration.

of periodic solutions allows to validate, for the state-of-the art model of flute-like instruments, the approach through orthogonal collocation and numerical continuation, and to begin to appreciate the benefits of such an approach. Hereafter, we extend the study to a more complete bifurcation diagram, in order to provide a better understanding of the instrument behaviour.

4.2 Analysis of the transition between registers

The phenomenon of "register change" is well-known by flute players: occurring while the musician blows harder in the instrument, it corresponds to a "jump" from a given note on the first register to another one on the second register whose frequency is approximately twice the first (that is to say, a jump of approximately one octave).

As highlighted in figure 11, representing the oscillation frequency of the acoustic velocity $v_{ac}(t)$ as a function of the dimensionless delay $\tilde{\tau}$, this phenomenon is also observed with time-domain simulations of the model, where the parameter $\tilde{\tau}$ now varies linearly. Starting from a frequency of 400 Hz at $\tilde{\tau} = 1.2$, a decrease of the delay (corresponding to an increase of the jet velocity U_j) leads to successive jumps to notes with higher frequencies. As observed experimentally (see for example [3]), the register changes are accompanied by hysteresis: starting from the arrival point of

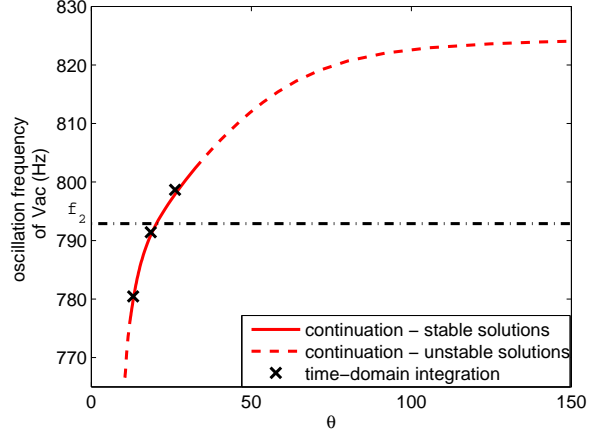


Figure 10: Oscillation frequency as a function of the reduced jet velocity θ for a single periodic solution branch. Superimposition of the results of numerical continuation and time-domain integration. The dark dot-dashed line indicates the second resonance frequency ($f_2 = \frac{\omega_2}{2\pi}$) of the resonator.

the decreasing ramp of delay $\tilde{\tau}$ and performing an increasing ramp of the delay also leads to jumps, but they occur at different delay values from those observed previously.

However, if this approach highlights the presence of register changes with hysteresis, it does not provide information about the cause of these jumps and of the associated hysteresis phenomenon. Moreover, as can be seen in figure 12, representing for the same simulations as in figure 11 the oscillation amplitude as a function of the dimensionless delay, the simulation results can be difficult to understand and interpret, due to the large number of observed regimes and "amplitude jumps".

The sensitivity to initial conditions make such an interpretation even more complicated: for the same parameters, a small change in the initial conditions of the state variables can result in a very different behaviour (periodic solution with different amplitude and frequency, but also non-periodic solutions).

The superimposition, in figures 13 and 14 of the bifurcation diagram and the results of simulations already presented above, provides a global overview of the different existing periodic regimes, and thus allows a better understanding of the observed phenomena. The bifurcation diagram highlights, for the range of the delay $\tilde{\tau}$ under investigation, the existence of five periodic solution

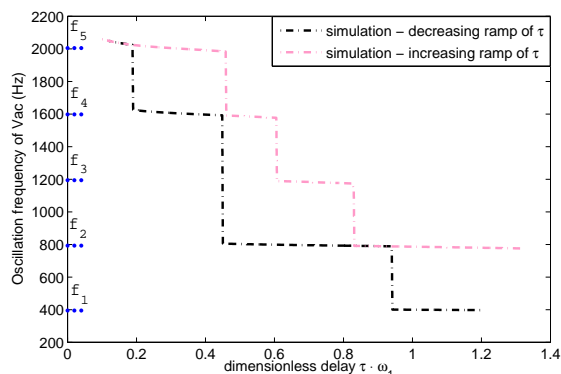


Figure 11: Oscillation frequency obtained through time-domain integration of the flute model for both a decreasing and an increasing ramp of the delay $\tilde{\tau}$. The lines of blue dots indicate the resonance frequencies of the resonator ($f_1 = \frac{\omega_1}{2\pi}$, $f_2 = \frac{\omega_2}{2\pi}$, $f_3 = \frac{\omega_3}{2\pi}$, $f_4 = \frac{\omega_4}{2\pi}$, $f_5 = \frac{\omega_5}{2\pi}$).

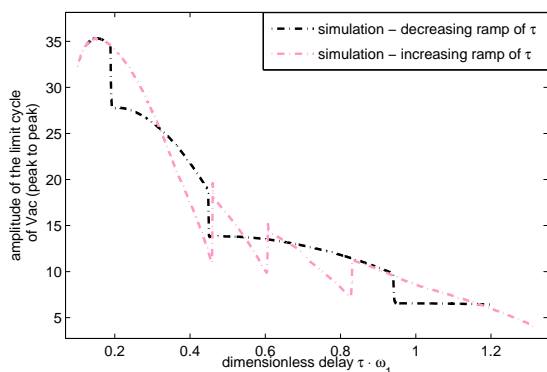


Figure 12: Oscillation amplitude obtained through time-domain integration of the flute model for both a decreasing and an increasing ramp of the delay $\tilde{\tau}$.

branches, corresponding to the five different registers, that is to say to oscillations on each (non uniform) mode of the resonator (see the third equation of system (1)). Stable and unstable parts of the branches are respectively represented by solid lines and dashed lines.

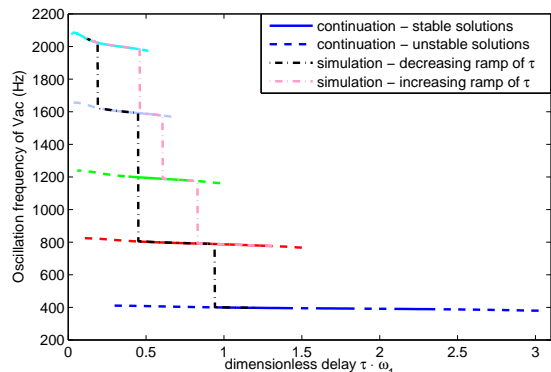


Figure 13: Oscillation frequency obtained through time-domain integration of the flute model for both a decreasing and an increasing ramp of the delay $\tilde{\tau}$, superimposed with the bifurcation diagram obtained through numerical continuation.

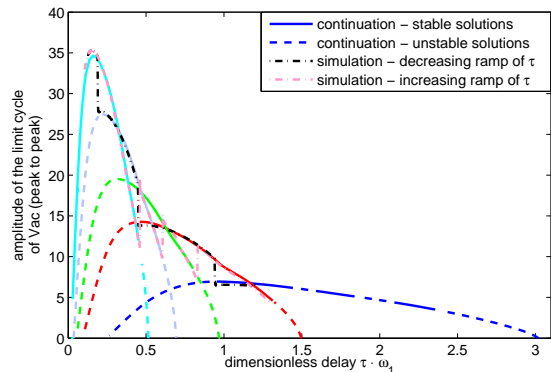


Figure 14: Oscillation amplitude obtained through time-domain simulation of the flute model for both a decreasing and an increasing ramp of the delay $\tilde{\tau}$, superimposed with the bifurcation diagram obtained through numerical continuation.

This comparison between the bifurcation diagram and simulations shows that the "jump" from a given register A to another register B is caused by the loss of stability (through a Neimark-Sacker bifurcation) of the branch of periodic solution corresponding to the register A. Such a bifurcation can lead to the birth of a quasiperiodic regime,

which would be called a *multiphonic sound* in a musical context, and whose generation mechanism in flute-like instruments is described more precisely in [22].

The confrontation between the bifurcation diagram and simulations also allows to explain the hysteresis phenomenon by the coexistence of several stable periodic solutions for a same value of the delay $\tilde{\tau}$. Let us consider the case of transition between registers 4 and 5 (corresponding respectively to oscillations at about $\omega_4/(2\pi) = 1600Hz$ and $\omega_5/(2\pi) = 2000Hz$): starting from the 4th register, at $\tilde{\tau} = 0.44$, a decrease of $\tilde{\tau}$ leads to a jump on the five register at $\tilde{\tau} = 0.19$. Starting an increasing ramp of the delay from this point, one observe that the system remains on the branch corresponding to the 5th register, until it becomes unstable, at $\tilde{\tau} = 0.45$.

In the same way, it can explain the fact that some regimes (for example the third register) are only observed, using time-domain integration, in the case of an increasing ramp of the delay, and not in the case of a decreasing ramp. Thereby, the bifurcation diagram allows us to predict, in the case of a quasi-static variation of the delay, both oscillation threshold and thresholds of register change. As such a prediction is impossible with the classical approach involving a linear analysis of the model (see for example [3]), it highlights the valuable contribution of the method. Indeed, if the analysis of the model linearised around the equilibrium solution allows to predict the thresholds corresponding to instabilities of the equilibrium solution (that is to say the birth of the periodic solution branches - see figure 14), it does not provide any information about stability of the emerging periodic solution. Nevertheless, as highlighted in figure 14, a periodic solution is not necessary stable at the birth of the branch, and the threshold predicted by linear analysis does not necessary correspond to the "observable" threshold of a given oscillation regime. As a consequence of thresholds prediction, a bifurcation diagram also predicts and explains hysteresis ranges, which is impossible through a linear analysis, and not necessary possible using time-domain simulations, due to the sensitivity to initial conditions, as underlined above. This is however a relevant information in the context of musical acoustics since it is related with how comfortable a musician feels when playing the instrument [3]. Indeed, an important hysteresis allows him to play

both *forte* on the first register and *piano* on the second register.

Thus, the bifurcation diagram, giving access to new kind of information (especially existence of unstable solutions, co-existence of multiple stable solutions, and oscillation amplitude and frequency of different periodic solutions of the nonlinear model), enables an easier interpretation of the simulation results (see figures 12 and 14), a more precise prediction of some characteristics of the different periodic regimes (especially their thresholds), and explains some aspects of the model behaviour observed in simulations, such as hysteresis associated to register changes.

5 Conclusion

Widely used in many scientific fields, methods dedicated to computation of periodic solutions of nonlinear dynamical systems have demonstrated, in several previous works [10, 11, 12, 17, 16], their benefits for the study of musical instruments. However, no available software (such as AUTO [8], Manlab [18], or DDE-Biftool [19]) is suitable for neutral delayed systems, involved in the modeling of flute-like instruments. The orthogonal collocation method has recently been adapted to such systems [23], allowing us to consider a study of the state-of-the-art model of flutes through numerical continuation.

The comparison between the results of orthogonal collocation coupled with numerical continuation algorithm and time-domain integration shows very good agreement in terms of oscillation amplitude and frequency, thresholds of the different periodic regimes, and waveforms. It thus allows the validation of this new approach to study flute-like instruments. Giving access to bifurcation diagram of the model, this method provides a more global knowledge of the model dynamics, and permits to explore more broadly the influence of the variation of a parameter. Thereby, it allows to explain and predict more precisely different aspects of the model behaviour, which can be related to some phenomena observed experimentally in flute-like instruments, such as register changes and associated hysteresis. Thus, the access to this more global knowledge of the model behaviour should allow to envisage an easier qualitative confrontation between numerical and experimental results.

Nevertheless, this method presents a number

of restrictions, and is thus not capable of replacing time-domain simulations entirely, but is a useful complement. Especially, one can only compute steady-state solutions, and there is no calculation of the transients, which are particularly important in the musician's playing. In the same way, this method only provides information about the behaviour of the model in the case of a quasi-static variation of the continuation parameter. Since recent studies [46] have highlighted the strong influence of the variation rate of a control parameter on the behaviour of a dynamical system, one can wonder about the validity of the bifurcation diagram in a musical context, where many control parameters vary continuously. Moreover, while orthogonal collocation can be extended to compute non-periodic solutions (such as for example quasiperiodic, intermittent or chaotic regimes), the software package used here is not currently suitable for such calculations.

A Reformulation of the model

Both to highlight its mathematical nature and to allow its implementation in DDE-Biftool and its extension for neutral systems, the model needs to be written as a first-order system: $\dot{x}(t) = f(x(t), x(t - \tau), \dot{x}(t - \tau), \lambda)$, with x the vector of state variables, and λ the set of parameters.

Starting from system (1), and writing the third equation in the time-domain leads to:

$$\begin{aligned} \eta(t) &= \frac{h}{U_j} e^{\alpha_i W} v_{ac}(t - \tau) \\ \Delta p(t) &= \frac{\rho \delta_d b U_j}{W} \frac{d}{dt} \left[\tanh \left(\frac{\eta(t) - y_0}{b} \right) \right] \\ &\quad - \frac{\rho}{2} \left(\frac{v_{ac}(t)}{\alpha_{vc}} \right)^2 \operatorname{sgn}(v_{ac}(t)) \\ V_{ac}(\omega) &= \left(\frac{a_0}{b_0 j \omega + c_0} + \sum_{k=1}^{p-1} \frac{a_k j \omega}{\omega_k^2 - \omega^2 + j \omega \frac{\omega_k}{Q_k}} \right) \cdot \Delta P(\omega) \end{aligned} \quad (15)$$

For each non uniform mode k , we define $V_{ac_k}(\omega)$ such as $V_{ac_k}(\omega) = \frac{a_k j \omega}{\omega_k^2 - \omega^2 + j \omega \frac{\omega_k}{Q_k}} \cdot \Delta P(\omega)$ (with k an integer such as $k \in [1; p - 1]$). In the same way, we define $V_{ac_0}(\omega) = \frac{a_0}{b_0 j \omega + c_0} \cdot \Delta P(\omega)$, such as one finally obtains $V_{ac} = V_{ac_0} + \sum_{k=1}^{p-1} V_{ac_k}$.

System (15) can thus be written as:

$$\begin{aligned} \eta(t) &= \frac{h}{U_j} e^{\alpha_i W} v_{ac}(t - \tau) \\ \Delta p(t) &= \frac{\rho \delta_d b U_j}{W} \frac{d}{dt} \left[\tanh \left(\frac{\eta(W, t) - y_0}{b} \right) \right] \\ &\quad - \frac{\rho}{2} \left(\frac{v_{ac}(t)}{\alpha_{vc}} \right)^2 \operatorname{sgn}(v_{ac}(t)) \\ V_{ac}(\omega) &= \sum_{k=0}^{p-1} V_{ac_k}(\omega) \\ V_{ac_0}(\omega) &= \left(\frac{a_0}{b_0 j \omega + c_0} \right) \cdot \Delta P(\omega) \\ V_{ac_1}(\omega) &= \left(\frac{a_1 j \omega}{\omega_1^2 - \omega^2 + j \omega \frac{\omega_1}{Q_1}} \right) \cdot \Delta P(\omega) \\ &\quad \vdots \\ V_{ac_{(p-1)}}(\omega) &= \left(\frac{a_{(p-1)} j \omega}{\omega_{(p-1)}^2 - \omega^2 + j \omega \frac{\omega_{(p-1)}}{Q_{(p-1)}}} \right) \\ &\quad \cdot \Delta P(\omega) \end{aligned} \quad (16)$$

Through an inverse Fourier transform, each expression V_{ac_k} (with $k \in [1; p - 1]$) can be written as:

$$\begin{aligned} \frac{d^2 v_{ac_k}(t)}{dt^2} + \frac{\omega_k}{Q_k} \cdot \frac{d v_{ac_k}(t)}{dt} + \omega_k^2 v_{ac_k}(t) \\ = a_k \frac{d \Delta p(t)}{dt} \end{aligned} \quad (17)$$

and the expression of V_{ac_0} becomes:

$$b_0 \cdot \frac{d v_{ac_0}(t)}{dt} + c_0 v_{ac_0}(t) = a_0 \Delta p(t) \quad (18)$$

The reinjection of the expressions of $\Delta p(t)$ and $\eta(t)$ leads to:

$$\begin{aligned}
v_{ac}(t) &= \sum_{k=0}^{p-1} v_{ac_k}(t) \\
\frac{dv_{ac_0}(t)}{dt} &= \frac{a_0 \rho \delta_d b U_j}{b_0 W} \frac{d}{dt} \left[\tanh \left(\frac{\eta(W, t) - y_0}{b} \right) \right] \\
&\quad - \frac{a_0 \rho}{2b_0} \frac{v_{ac}^2}{\alpha_{vc}^2} \operatorname{sgn}(v_{ac}) - c_0 v_{ac_0}(t) \\
\frac{d^2 v_{ac_k}(t)}{dt^2} &= \frac{a_k \rho \delta_d b U_j}{W} \frac{d^2}{dt^2} \left\{ \tanh \left[\frac{h e^{\alpha_i W}}{b U_j} \right. \right. \\
&\quad \left. \left. \cdot v_{ac}(t - \tau) - \frac{y_0}{b} \right] \right\} \\
&\quad - a_k \frac{d}{dt} \left[\frac{\rho}{2} \left(\frac{v_{ac}}{\alpha_{vc}} \right)^2 \operatorname{sgn}(v_{ac}) \right] \\
&\quad - \frac{\omega_k}{Q_k} \frac{dv_{ac_k}(t)}{dt} - \omega_k^2 v_{ac_k}(t).
\end{aligned} \tag{19}$$

To improve numerical conditioning of the problem, we define the following dimensionless variables:

$$\begin{aligned}
\tilde{t} &= \omega_1 t \\
\tilde{v}_k(\tilde{t}) &= \frac{h e^{\alpha_i W}}{b U_j} v_{ac_k}(\tilde{t})
\end{aligned} \tag{20}$$

Noting $\dot{\tilde{v}}(\tilde{t})$ and $\ddot{\tilde{v}}(\tilde{t})$ respectively the first and second order derivative of $\tilde{v}(\tilde{t})$ with respect to the dimensionless time \tilde{t} , one finally obtains:

$$\begin{aligned}
\dot{\tilde{v}}_0(\tilde{t}) &= \frac{a_0 \rho \delta_d h e^{\alpha_i W}}{W b_0} \sum_{i=0}^{p-1} \dot{\tilde{v}}_i(\tilde{t} - \tilde{\tau}) \\
&\quad \left\{ 1 - \tanh^2 \left[\sum_{i=0}^{p-1} \tilde{v}_i(\tilde{t} - \tilde{\tau}) - \frac{y_0}{b} \right] \right\} \\
&\quad - \frac{a_0 \rho b W}{2 b_0 \alpha_{vc}^2 h e^{\alpha_i W} \gamma \tilde{\tau}} \sum_{i=0}^{p-1} \tilde{v}_i(\tilde{t}) \\
&\quad \operatorname{abs} \left[\sum_{i=0}^{p-1} \tilde{v}_i(\tilde{t}) \right] - \frac{c_0}{b_0 \omega_1} \tilde{v}_0(\tilde{t}) \\
\ddot{\tilde{v}}_k(\tilde{t}) &= \frac{a_k \rho \delta_d h e^{\alpha_i W}}{W} \sum_{i=0}^{p-1} \ddot{\tilde{v}}_i(\tilde{t} - \tilde{\tau}) \\
&\quad \left\{ 1 - \tanh^2 \left[\sum_{i=0}^{p-1} \tilde{v}_i(\tilde{t} - \tilde{\tau}) - \frac{y_0}{b} \right] \right\} \\
&\quad - \frac{2 a_k \rho \delta_d h e^{\alpha_i W}}{W} \left(\sum_{i=0}^{p-1} \dot{\tilde{v}}_i(\tilde{t} - \tilde{\tau}) \right)^2 \\
&\quad \operatorname{tanh} \left[\sum_{i=0}^{p-1} \tilde{v}_i(\tilde{t} - \tilde{\tau}) - \frac{y_0}{b} \right] \\
&\quad \left\{ 1 - \tanh^2 \left[\sum_{i=0}^{p-1} \tilde{v}_i(\tilde{t} - \tilde{\tau}) - \frac{y_0}{b} \right] \right\} \\
&\quad - \frac{a_k \rho b W}{2 \alpha_{vc}^2 h e^{\alpha_i W} \gamma \tilde{\tau}} \sum_{i=0}^{p-1} \dot{\tilde{v}}_i(\tilde{t}) \\
&\quad \operatorname{abs} \left[\sum_{i=0}^{p-1} \tilde{v}_i(\tilde{t}) \right] - \left(\frac{b W}{\gamma \tilde{\tau} \alpha_{vc} h e^{\alpha_i W}} \right)^2 \\
&\quad \frac{a_k \rho \omega_1}{2} \sum_{i=0}^{p-1} \tilde{v}_i(\tilde{t}) \sum_{i=0}^{p-1} \dot{\tilde{v}}_i(\tilde{t}) \\
&\quad \operatorname{sgn} \left[\sum_{i=0}^{p-1} \tilde{v}_i(\tilde{t}) \right] - \left(\frac{\omega_k}{\omega_1} \right)^2 \tilde{v}_k(\tilde{t}) \\
&\quad - \frac{\omega_k}{\omega_1 Q_k} \dot{\tilde{v}}_k(\tilde{t})
\end{aligned} \tag{21}$$

$$\forall k \in [1; 2; \dots; p-2; p-1].$$

The definition of the variables: $\tilde{z}_k(\tilde{t}) = \dot{\tilde{v}}_k(\tilde{t})$ finally allow to reduce system (21) to a first-order system:

$$\begin{aligned}
\dot{\tilde{v}}_0(\tilde{t}) &= \frac{a_0 \rho \delta_d h e^{\alpha_i W}}{W b_0} \sum_{i=0}^{p-1} \tilde{z}_i(\tilde{t} - \tilde{\tau}) \\
&\quad \left\{ 1 - \tanh^2 \left[\sum_{i=0}^{p-1} \tilde{v}_i(\tilde{t} - \tilde{\tau}) - \frac{y_0}{b} \right] \right\} \\
&\quad - \frac{a_0 \rho b W}{2 b_0 \alpha_{vc}^2 h e^{\alpha_i W} \gamma \tilde{\tau}} \sum_{i=0}^{p-1} \tilde{v}_i(\tilde{t}) \\
&\quad \text{abs} \left[\sum_{i=0}^{p-1} \tilde{v}_i(\tilde{t}) \right] - \frac{c_0}{b_0 \omega_1} \tilde{v}_0(\tilde{t}) \\
\dot{\tilde{v}}_k(\tilde{t}) &= \tilde{z}_k(\tilde{t}) \\
\dot{\tilde{z}}_k(\tilde{t}) &= \frac{a_k \rho \delta_d h e^{\alpha_i W}}{W} \sum_{i=0}^{p-1} \dot{\tilde{z}}_i(\tilde{t} - \tilde{\tau}) \\
&\quad \left\{ 1 - \tanh^2 \left[\sum_{i=0}^{p-1} \tilde{v}_i(\tilde{t} - \tilde{\tau}) - \frac{y_0}{b} \right] \right\} \\
&\quad - \frac{2 a_k \rho \delta_d h e^{\alpha_i W}}{W} \left(\sum_{i=0}^{p-1} \tilde{z}_i(\tilde{t} - \tilde{\tau}) \right)^2 \\
&\quad \tanh \left[\sum_{i=0}^{p-1} \tilde{v}_i(\tilde{t} - \tilde{\tau}) - \frac{y_0}{b} \right] \\
&\quad \left\{ 1 - \tanh^2 \left[\sum_{i=0}^{p-1} \tilde{v}_i(\tilde{t} - \tilde{\tau}) - \frac{y_0}{b} \right] \right\} \\
&\quad - \frac{a_k \rho b W}{2 \alpha_{vc}^2 h e^{\alpha_i W} \gamma \tilde{\tau}} \sum_{i=0}^{p-1} \tilde{z}_i(\tilde{t}) \\
&\quad \text{abs} \left[\sum_{i=0}^{p-1} \tilde{v}_i(\tilde{t}) \right] - \left(\frac{b W}{\gamma \tilde{\tau} \alpha_{vc} h e^{\alpha_i W}} \right)^2 \\
&\quad \frac{a_k \rho \omega_1}{2} \sum_{i=0}^{p-1} \tilde{v}_i(\tilde{t}) \sum_{i=0}^{p-1} \tilde{z}_i(\tilde{t}) \\
&\quad \text{sgn} \left[\sum_{i=0}^{p-1} \tilde{v}_i(\tilde{t}) \right] - \left(\frac{\omega_k}{\omega_1} \right)^2 \tilde{v}_k(\tilde{t}) \\
&\quad - \frac{\omega_k}{\omega_1 Q_k} \tilde{z}_k(\tilde{t})
\end{aligned} \tag{22}$$

$\forall k \in [1; 2; \dots; p-2; p-1]$, with p the total number of modes.

References

- [1] J W Coltman. Time-domain simulation of the flute. *Journal of the Acoustical Society of America*, 92:69–73, 1992.
- [2] J W Coltman. Jet offset, harmonic content, and warble in the flute. *Journal of the Acoustical Society of America*, 120(4):2312–2319, 2006.
- [3] R Auvray, B Fabre, and P Y Lagrée. Regime change and oscillation thresholds in recorder-like instruments. *Journal of the Acoustical Society of America*, 131(4):1574–1585, 2012.
- [4] R T Schumacher. Self-sustained oscillations of organ flue pipes: an integral equation solution. *Acustica*, 39:225–238, 1978.
- [5] N H Fletcher. Sound production by organ flue pipes. *Journal of the Acoustical Society of America*, 60(4):926–936, 1976.
- [6] M Nakhla and J Vlach. A piecewise harmonic balance technique for determination of periodic response of nonlinear systems. *Circuits and Systems, IEEE Transactions on*, 23(2):85–91, 1976.
- [7] E J Doedel. Lecture notes on numerical analysis of nonlinear equations. In *Numerical Continuation Methods for dynamical systems*, pages 1–49. Springer, 2007.
- [8] E J Doedel. AUTO: A program for automatic bifurcation analysis of autonomous systems. *Congressus Numerantium*, 30:265–284, 1981.
- [9] B Krauskopf, H M Osinga, and J Galan-Vioque. *Numerical continuation methods for dynamical systems*. Springer, 2007.
- [10] J Gilbert, J Kergomard, and E Ngoya. Calculation of the steady-state oscillations of a clarinet using the harmonic balance technique. *Journal of the Acoustical Society of America*, 86(1):35–41, 1989.
- [11] C Fritz, S Farner, and J Kergomard. Some aspects of the harmonic balance method applied to the clarinet. *Applied Acoustics*, 65:1155–1180, 2004.
- [12] S Farner, C Vergez, J Kergomard, and A Lizée. Contribution to harmonic balance calculations of self-sustained periodic oscillations with focus on single-reed instruments. *The Journal of the Acoustical Society of America*, 119:1794, 2006.
- [13] J P Dalmont and J Gilbert, Jand Kergomard. Reed instruments, from small to large amplitude periodic oscillations and the

- helmholtz motion analogy. *Acta Acustica united with Acustica*, 86(4):671–684, 2000.
- [14] L Menguy and J Gilbert. Weakly nonlinear gas oscillations in air-filled tubes; solutions and experiments. *Acta Acustica united with Acustica*, 86(5):798–810, 2000.
- [15] J Gilbert, L Menguy, and M Campbell. A simulation tool for brassiness studies. *The Journal of the Acoustical Society of America*, 123:1854, 2008.
- [16] S Karkar, C Vergez, and B Cochelin. Toward the systematic investigation of periodic solutions in single reed woodwind instruments. In *Proceedings of the 20th International Symposium on Music Acoustics*, Sydney, Australia, August 2010.
- [17] S Karkar, C Vergez, and B Cochelin. Oscillation threshold of a clarinet model: a numerical continuation approach. *Journal of the Acoustical Society of America*, 131(1):698–707, 2012.
- [18] B Cochelin and C Vergez. A high order purely frequency-based harmonic balance formulation for continuation of periodic solutions. *Journal of Sound and Vibration*, 324:243–262, 2009.
- [19] K Engelborghs. DDE Biftool: a Matlab package for bifurcation analysis of delay differential equations. Technical report, Katholieke Universiteit Leuven, 2000.
- [20] A Dhooge, W Govaerts, and Y A Kuznetsov. Matcont: a matlab package for numerical bifurcation analysis of odes. *ACM Transactions on Mathematical Software (TOMS)*, 29(2):141–164, 2003.
- [21] S Junca and B Lombard. Interaction between periodic elastic waves and two contact nonlinearities. *Mathematical Models and Methods in Applied Sciences*, 22(04), 2012.
- [22] S Terrien, C Vergez, and B Fabre. Flute-like musical instruments: A toy model investigated through numerical continuation. *Journal of sound and vibration*, 332(1):3833–3848, 2013.
- [23] D Barton, B Krauskopf, and R E Wilson. Collocation schemes for periodic solutions of neutral delay differential equations. *Journal of Difference Equations and Applications*, 12(11):1087–1101, 2006.
- [24] J W S Rayleigh. *The theory of sound second edition*. New York, Dover, 1894.
- [25] P de la Cuadra, C Vergez, and B Fabre. Visualization and analysis of jet oscillation under transverse acoustic perturbation. *Journal of Flow Visualization and Image Processing*, 14(4):355–374, 2007.
- [26] A Nolle. Sinuous instability of a planar jet: propagation parameters and acoustic excitation. *Journal of the Acoustical Society of America*, 103:3690–3705, 1998.
- [27] M P Verge, R Caussé, B Fabre, A Hirschberg, A P J Wijnands, and A van Steenbergen. Jet oscillations and jet drive in recorder-like instruments. *Acta Acustica united with Acustica*, 2:403–419, 1994.
- [28] J W Coltman. Jet drive mechanisms in edge tones and organ pipes. *Journal of the Acoustical Society of America*, 60(3):725–733, 1976.
- [29] M P Verge, A Hirschberg, and R Caussé. Sound production in recorder-like instruments. ii. a simulation model. *Journal of the Acoustical Society of America*, 101(5):2925–2939, 1997.
- [30] A Chaigne and J Kergomard. *Acoustique des instruments de musique (Acoustics of musical instruments)*, chapter 10. Belin (Echelles), 2008.
- [31] P de la Cuadra. *The sound of oscillating air jets: Physics, modeling and simulation in flute-like instruments*. PhD thesis, Stanford University, 2005.
- [32] C Ségoufin, B Fabre, M P Verge, A Hirschberg, and A P J Wijnands. Experimental study of the influence of the mouth geometry on sound production in a recorder-like instrument: Windway length and chamfers. *Acta Acustica united with Acustica*, 86(4):649–661, 2000.
- [33] B Fabre and A Hirschberg. Physical modeling of flue instruments: A review of lumped models. *Acta Acustica united with Acustica*, 86:599–610, 2000.

- [34] B Fabre, A Hirschberg, and A P J Wijnands. Vortex shedding in steady oscillation of a flue organ pipe. *Acta Acustica united with Acustica*, 82(6):863–877, 1996.
- [35] S Terrien, R Auvray, B Fabre, P Y Lagrée, and C Vergez. Numerical resolution of a physical model of flute-like instruments: comparison between different approaches. In *Proceedings of Acoustics 2012*, Nantes, France, 2012.
- [36] R Szalai. Knut: A continuation and bifurcation software for delay-differential equations, 2009. Available online at: <http://gitorious.org/knut/pages/Home> (accessed 5 July 2013).
- [37] D Barton, B Krauskopf, and R E Wilson. Bifurcation analysis tools for neutral delay equations: a case study. In *6th IFAC conference on Time-Delay Systems*, 2006.
- [38] K Engelborghs, T Luzyanina, K J In’t Hout, and D Roose. Collocation methods for the computation of periodic solutions of delay differential equations. *SIAM Journal on Scientific Computing*, 22(5):1593–1609, 2000.
- [39] K Engelborghs, T Luzyanina, and D Roose. Numerical bifurcation analysis of delay differential equations using DDE-Biftool. *ACM Transactions on Mathematical Software*, 28(1):1–21, 2002.
- [40] D Breda, S Maset, and R Vermiglio. Pseudospectral approximation of eigenvalues of derivative operators with non-local boundary conditions. *Applied Numerical Mathematics*, 56(3-4):318–331, March 2006.
- [41] A H Nayfeh and B Balachandran. *Applied Nonlinear Dynamics*. Wiley, 1995.
- [42] H B Keller. Numerical solution of bifurcation and nonlinear eigenvalue problems. *Applications of bifurcation theory*, pages 359–384, 1977.
- [43] M Meissner. Aerodynamically excited acoustic oscillations in cavity resonator exposed to an air jet. *Acta Acustica united with Acustica*, 88(2):170–180, 2002.
- [44] J W Coltman. Resonance and sounding frequencies of the flute. *Journal of the Acoustical Society of America*, 40(1):99–107, 1966.
- [45] N Giordano. Direct numerical simulation of a recorder. *Journal of the Acoustical Society of America*, 133(2):1111–1118, 2013.
- [46] B Bergeot, A Almeida, C Vergez, and B Gazengel. Prediction of the dynamic oscillation threshold in a clarinet model with a linearly increasing blowing pressure. *Nonlinear Dyn*, 73(1-2):521–534, July 2013.